The Journal of Chemical Physics

A lattice Boltzmann model for self-diffusiophoretic particles near and at liquid–liquid interfaces

Cite as: J. Chem. Phys. **156**, 224105 (2022); https://doi.org/10.1063/5.0087203
Submitted: 02 February 2022 • Accepted: 02 May 2022 • Published Online: 09 June 2022

Lucas S. Palacios, Andrea Scagliarini and Ignacio Pagonabarraga

The Journal of Chemical Physics ARTICLE scitation.org/journal/jcp

A lattice Boltzmann model for self-diffusiophoretic particles near and at liquid–liquid interfaces

Cite as: J. Chem. Phys. 156, 224105 (2022); doi: 10.1063/5.0087203
Submitted: 2 February 2022 • Accepted: 2 May 2022 •
Published Online: 9 June 2022

Lucas S. Palacios,[1] Andrea Scagliarini,[2,3] and Ignacio Pagonabarraga[4,5,6,a)]

AFFILIATIONS

[1] Institute for Bioengineering of Catalonia (IBEC), The Barcelona Institute of Science and Technology (BIST), Baldiri i Reixac 10-12, 08028 Barcelona, Spain
[2] Istituto per le Applicazioni del Calcolo, CNR–Via dei Taurini 19, 00185 Rome, Italy
[3] INFN, Sezione di Roma "Tor Vergata," Via della Ricerca Scientifica 1, 00133 Rome, Italy
[4] Departament de Física de la Materia Condensada, Universitat de Barcelona, Carrer Martí i Franqués 1, 08028 Barcelona, Spain
[5] Universitat de Barcelona Institute of Complex Systems (UBICS), Universitat de Barcelona, 08028 Barcelona, Spain
[6] CECAM, Centre Europeén de Calcul Atomique et Moléculaire, Ecole Polytechnique Fédérale de Lausanne (EPFL), Avenue Forel 2, 1015 Lausanne, Switzerland

[a)] **Author to whom correspondence should be addressed:** ipagonabarraga@ub.edu

ABSTRACT

We introduce a novel mesoscopic computational model based on a multiphase-multicomponent lattice Boltzmann method for the simulation of self-phoretic particles in the presence of liquid–liquid interfaces. Our model features fully resolved solvent hydrodynamics, and, thanks to its versatility, it can handle important aspects of the multiphysics of the problem, including particle wettability and differential solubility of the product in the two liquid phases. The method is extensively validated in simple numerical experiments, whose outcome is theoretically predictable, and then applied to the study of the behavior of active particles next to and trapped at interfaces. We show that their motion can be variously steered by tuning relevant control parameters, such as the phoretic mobilities, the contact angle, and the product solubility.

I. INTRODUCTION

Artificial micromotors have gained an ever-growing interest, in recent years, as biomimetic devices and for their manifold microfluidic applications.[1] Being able to convert ambient energy into autonomous motion, they fall in the realm of active matter.[2]

A paradigmatic example of model micromotors is provided by self-phoretic particles (SPPs), which self-propel exploiting the phenomenon of colloidal phoresis[3] in the inhomogeneous solute distribution generated by a chemical reaction or a phase transition locally occurring at their surfaces. SPPs include Janus metallic rods[4] and catalytic[1,5,6] and light-activated Janus colloids,[7,8] among others (see also Refs. 9–11 and references therein for reviews). Extensively studied are suspensions of platinum coated, micrometer-sized polymeric spheres in an aqueous solution of hydrogen peroxide; the latter undergoes a decomposition reaction, catalyzed by platinum, into water and oxygen. For this reason, in what follows, we will often refer to the solute as oxygen; however, as it will be made clear, the model simply requires the generation and diffusion of a scalar field. The approach is, therefore, more general and can simulate SPPs based on different mechanisms, such as the critical water–lutidine demixing[12] or even self-thermophoretic colloids.[13,14]

Despite the consistent body of theoretical, computational, and experimental works witnessed, many questions remain still unanswered in the physics of SPPs, especially when it comes to more complex environments than the bulk of a fluid, as, e.g., in the presence of interfaces.[11] As a matter of fact, how the motion of these active particles could be modified or steered by the presence of an interface is not yet totally understood. Recent studies have focused on solid–liquid interfaces,[15–17] liquid–liquid interfaces,[18–21] or even on a combination of both,[22] but a theoretical/computational approach taking into account hydrodynamics and a thermodynamically

consistent modeling of the multiphase solute–solvent–particle system is so far missing. Indeed, liquid–liquid interfaces add extra degrees of freedom to the system, owing to their deformability and to the solid phase wetting properties, thus significantly enriching the particle dynamics. Given also the intrinsic out-of-equilibrium physics of active particles, it appears clear how modeling may represent a challenging task.

In this paper, we propose a mesoscopic numerical model based on a multiphase lattice Boltzmann method, featuring a free energy functional that depends on two phase fields, describing the two immiscible component mixture (e.g., oil and water) and the product (oxygen), respectively, and contains a novel coupling between them, allowing for a tunable affinity of the solute for the two phases. The suspended solid particles are endowed with the capability of performing diffusiophoretic motion and generating a solute field, which stems from the activity of the catalytic site. The uniqueness of the method resides in the capability of handling at the same time solvent hydrodynamics and particle–solute interactions, giving rise to self-propulsion, wettability, and preferential solubility of oxygen, which can, in general, accumulate more in one of the two liquid phases, thus allowing us to simulate different combination of immiscible fluids.

This paper is organized as follows: In Sec. II, the thermo-hydrodynamic model is introduced and tested together with the description of the fluid–solid coupling and of the implementation of the self-diffusiophoresis. In Sec. III, we present the model validation against controlled setups, starting with that of an isolated SPP in a single phase fluid and then moving to the case of mixtures, distinguishing between active and inactive particles, in order to disentangle the effects of capillary and phoretic forces. We report results showing that the relative position and orientation of a self-phoretic Janus particle and an interface depend, in a non-trivial way, on wettability, phoretic mobilities, and oxygen solubility. Our findings suggest, then, that a proper tuning of such parameters may enable the guidance of active particles in non-homogeneous fluid media. Conclusions and perspectives are drawn in Sec. IV

II. COMPUTATIONAL MODEL

A suspension of active particles in the presence of liquid–liquid interfaces consists of a fluid phase (solvents + solute) and a solid phase (the active particles). To model such a multiphase (and multicomponent) system, we resort to a mesoscopic approach based on the lattice Boltzmann (LB) method[23–26] in the phase field formulation.[27–29]

A. Phase field model: The free energy functional

The fluid phase is a ternary mixture made of two immiscible liquids (say, water and oil) and a solute, which is the product of the reaction occurring at the catalytic site on the particle surface (the oxygen). We associate with the water–oil system a scalar field $\psi(\mathbf{r},t)$ standing for the local composition, that is, $\psi = \frac{\rho_W-\rho_O}{\rho_W+\rho_O}$, where ρ_W and ρ_O are the density fields of water and oil, respectively. As in the standard Cahn–Hilliard theory,[30] the thermodynamics of the oil–water mixture is controlled by a quartic in ψ double-well free energy density of Landau type, $f_{\mathrm{OW}}[\psi] = \frac{A}{4}\psi^4 + \frac{B}{2}\psi^2$ (with $A > 0$ and $B < 0$). This free energy has to be extended to embrace the dynamics of the oxygen, that is, in principle, miscible with each of the two other components; therefore, we need to add a term characterized by a single minimum that disregards the energetic cost associated with the concentration gradients[31] such that in the case of a single component solvent ($f_{\mathrm{OW}} = 0$ identically), a diffusive equation for the solute is recovered. A simple parabolic potential is appropriate to this aim (as we will show shortly), namely, $f^{(0)}_{O_2}[\phi] = \frac{C}{2}\phi^2$ $(C > 0)$, having introduced the field $\phi(\mathbf{r},t)$. In actual systems, though, the oxygen may display, in general, a greater affinityzz for one of the two liquids (it can be more soluble in water than in oil, or vice versa). To account for this preferential concentration, an "interaction" term, coupling ϕ and ψ, has to be included. We propose to do so by simply shifting the global minimum of $f^{(0)}_{O_2}$ in $\phi = 0$ to a ψ-dependent minimum, i.e., $f^{(0)}_{O_2}[\phi] = \frac{C}{2}\phi^2 \to f_{O_2}[\phi,\psi] = \frac{C}{2}(\phi-\phi_0(\psi))^2$. For $\phi_0(\psi)$, we choose the form $\phi_0(\psi) = \phi_b + E\tanh(\psi)$, where the parameter E tunes the oxygen solubility and ϕ_b sets the average oxygen concentration. The full free energy functional then reads

$$F[\psi,\phi] = \int \mathbf{dr}\left[\frac{A}{4}\psi^4 + \frac{B}{2}\psi^2 + \frac{\kappa}{2}|\nabla\psi|^2 + \frac{C}{2}(\phi - E\tanh(\psi) - \phi_{b0})^2\right]. \quad (1)$$

Hereafter, we set $B = -A$ such that the ψ minima, corresponding to the bulk water and oil phases, are located in $\psi = \pm 1$. The minimization of the functional (1) yields the chemical potentials $\mu_\phi = \frac{\delta F}{\delta\phi}$ and $\mu_\psi = \frac{\delta F}{\delta\psi}$,

$$\left.\begin{aligned}\mu_\phi &= C(\phi - E\tanh(\psi) - \phi_{b0})\\ \mu_\psi &= A(\psi^3-\psi) - \kappa\nabla^2\psi - CE\frac{(\phi - E\tanh(\psi) - \phi_{b0})}{\cosh^2(\psi)}\end{aligned}\right\}. \quad (2)$$

The dynamics of the ternary mixture system is, then, described by the following equations:

$$\left.\begin{aligned}\partial_t\phi + \nabla\cdot(\boldsymbol{u}\phi) &= D_\phi\nabla^2(\phi-\phi_0(\psi)) + \mathscr{D}_\phi - k_d(\phi-\phi_0(\psi))\\ \partial_t\psi + \nabla\cdot(\boldsymbol{u}\psi) &= D_\psi\nabla^2\left(\psi^3 - \psi - \frac{\kappa}{A}\nabla^2\psi - E\frac{\phi-\phi_0(\psi)}{\cosh^2(\psi)}\right)\end{aligned}\right\}, \quad (3)$$

where $D_\phi = C\,M_\phi$ and $D_\psi = A\,M_\psi$ are the diffusivities for the oxygen and the water–oil mixture, respectively, and M_ϕ and M_ψ are the mobility constants for ϕ and ψ. The equation for ϕ has been equipped with a source term, $\mathscr{D}_\phi$, that accounts for the generation of oxygen in a reaction catalyzed by the particles (see Sec. II B for further details). This production needs to be balanced by a sink term, $k_d(\phi-\phi_0(\psi))$, in order to allow the attainment of a steady state. Physically, the sink mimics the degradation of the production or its loss in the environment.[31] Figure 1 displays the effect of changing the solubility parameter from negative to positive values by plotting the average oxygen concentration, $\langle\phi\rangle_{O,W}$, in oil or water as a function of E at equilibrium and in the absence of particles (hence of oxygen production). Since, by virtue of Eq. (2), the

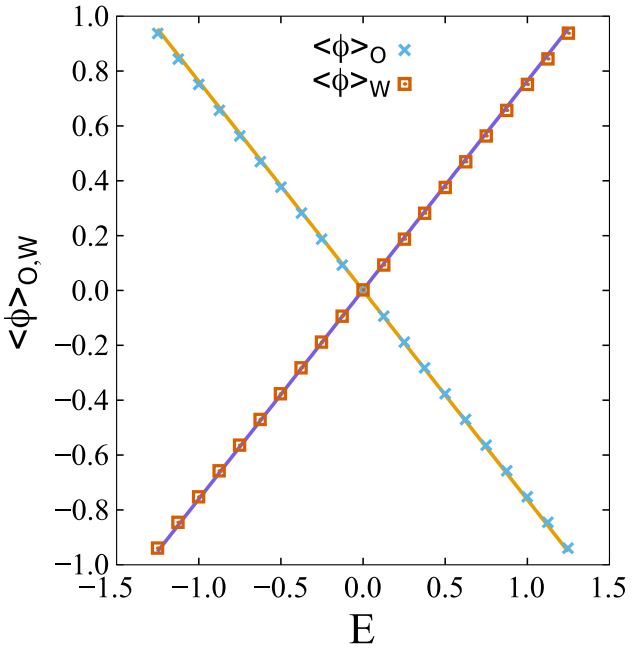

FIG. 1. Equilibrium oxygen concentration, averaged over the water (orange squares) and oil (blue crosses) phases, as a function of the E parameter. The solid lines represent the expectations from the thermodynamic model, $\langle\phi\rangle_{W,O} \approx \pm E\tanh(1)$, where the positive/negative sign corresponds to water/oil and is depicted in violet/yellow. The simulation were run with $\phi_{b0} = 0$.

equilibrium profile of ϕ is $\phi = E\tanh(\psi)$ (the background value having been set to zero here, $\phi_b = 0$), the average, up to terms of infinitesimal order in ξ/L (ξ being the interface width and L the system size), is $\langle\phi\rangle_{W,O} \approx \pm E\tanh(1)$, where the positive/negative sign corresponds to the average being taken over the water or oil phase, respectively; this prediction is reported in Fig. 1 with solid lines and agrees well with the numerical data.

B. Particles

Particles are modeled as solid spheres defined by a set of boundary "links" between inner and outer nodes. The fluid–solid coupling is realized by means of the so-called "bounce-back-on-links" algorithm that guarantees the proper momentum–torque exchange between particles and solvent.[32–36] Colloidal phoresis is introduced by imposing at the particle surface an effective slip velocity profile that depends on the local solute concentration[3] as

$$\boldsymbol{v}_s = \mu(\boldsymbol{r}_s)(\mathbf{1} - \hat{\boldsymbol{n}}\times\hat{\boldsymbol{n}})\cdot\nabla\phi, \tag{4}$$

where $\boldsymbol{r}_s$ is a point on the surface of the particle, $\hat{\boldsymbol{n}}(\boldsymbol{r}_s)$ is the normal to the surface in $\boldsymbol{r}_s$, and $\mu(\boldsymbol{r}_s)$ is the phoretic mobility at $\boldsymbol{r}_s$, which carries the molecular details of the solute–colloid interaction.[3] As a consequence, in the presence of concentration gradients, particles gain a net propulsion velocity $\boldsymbol{V}_p \sim -\mu\nabla\phi$ [for uniform phoretic mobility, $\mu(\boldsymbol{r}_s) \equiv \mu$]; hence, if $\mu < 0$, they are attracted by the solute, else if $\mu > 0$, they are repelled. To achieve self-propulsion, particles are, then, endowed with the property of generating the solute;[37] this is done by simply adding a production term that injects ϕ with a given rate at nodes neighboring the particles surfaces, thus modeling the catalytic activity of *Pt*-coated colloids. In particular, a Janus activity profile is chosen,

$$\Pi(\boldsymbol{r}_s) = \begin{cases} \alpha & \text{if } \hat{\boldsymbol{m}}\cdot\hat{\boldsymbol{n}}(\boldsymbol{r}_s) \le 0, \\ 0 & \text{if } \hat{\boldsymbol{m}}\cdot\hat{\boldsymbol{n}}(\boldsymbol{r}_s) > 0, \end{cases} \tag{5}$$

where α is the constant production rate and $\hat{\boldsymbol{m}}$ is the particle characteristic unit vector [see the sketch in Fig. 2(a)]. Note that the superposition of such activities associated with various particles is precisely what gives rise to the production term $\mathscr{D}_\phi$ appearing in Eq. (3). Analogously, for the phoretic mobility $\mu(\boldsymbol{r}_s)$, we set

$$\mu(\boldsymbol{r}_s) = \begin{cases} \mu_- & \text{if } \hat{\boldsymbol{m}}\cdot\hat{\boldsymbol{n}}(\boldsymbol{r}_s) \le 0, \\ \mu_+ & \text{if } \hat{\boldsymbol{m}}\cdot\hat{\boldsymbol{n}}(\boldsymbol{r}_s) > 0. \end{cases} \tag{6}$$

For an isolated Janus particle with the above activity and mobility profiles, we expect a motion with constant velocity of magnitude[37–39]

$$v_p = \frac{|(\mu_+ + \mu_-)|\alpha}{8D_\phi}. \tag{7}$$

When solid surfaces are involved, the presence of a three-phase contact line calls for a specific treatment of the interaction of the two liquids with the solid boundaries. Contact lines are relevant in various experimental contexts, where they play a crucial role, e.g., in the guidance of the motion of active particles.[22] A solid–liquid interaction determines also the particle wetting properties, and it is, therefore, needed even when confining walls are absent, as in the cases studied here. An extra boundary term is, then, added to the free energy functional,

$$F_{\text{tot}}[\phi,\psi] = F[\phi,\psi] + \int_S H\psi(\boldsymbol{r}_s)d\boldsymbol{r}_s, \tag{8}$$

where the integral is over the solid surface. The parameter H controls the wetting through the following boundary condition that can be derived by minimization of the surface term in (8),

$$H = \kappa|\nabla\psi\cdot\hat{\boldsymbol{n}}|, \tag{9}$$

and therefore, it sets the particle contact angle θ_c, to which it is related by[40]

$$\cos(\theta_c) = \frac{1}{2}\left[-(1-h)^{3/2} + (1+h)^{3/2}\right], \tag{10}$$

where $h = H\sqrt{1/(\kappa A)}$.

To the best of our knowledge, our method is the first implementing self-diffusiophoresis of active particles in multiphase fluids with the effective slip velocity formulation, which is, as a matter of fact, the only way to properly deal with the physical scale separation of the phenomena involved.

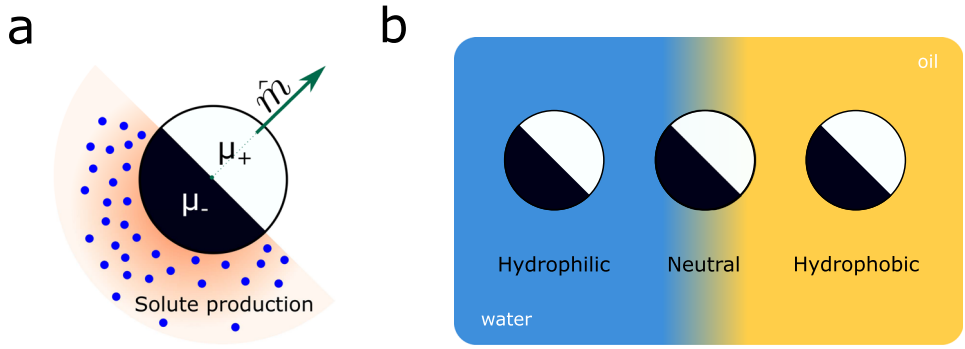

FIG. 2. (a) Sketch of a spherical self-diffusiophoretic particle. The particle is characterized by a Janus profile of both the activity (it produces solute only over one hemisphere) and the phoretic mobility, see Eqs. (5) and (6) (b) Active particle in the presence of an interface: depending on the value of the contact angle, θ_c, it tends to stay preferentially in the bulk of the water phase ($\theta_c > 90°$), of the oil phase ($\theta_c < 90°$), or adsorbed at the interface ($\theta_c = 90°$).

C. Numerical details

We numerically simulate the model just introduced on three-dimensional periodic lattices of sizes ranging between 32^3 to $64 \times 96 \times 96$ (with unit spacing, $\Delta x = 1$). The two liquids have the same kinematic viscosity, equal to $\nu = 1/6$, and the same density $\rho = 1$ given in lattice Boltzmann units as the other parameters hereafter (unless differently specified). The free energy parameters are set to $A = C = 0.0625$, $\kappa = 0.04$, such that the surface tension is $\sigma = (2/3)\sqrt{2\kappa A} \approx 0.047$, and the mobilities are $M_\psi = 0.4$ and $M_\phi = 0.8$, giving the diffusion coefficients $D_\psi = 0.025$ and $D_\phi = 0.05$. The particle radius is fixed to $R = 4.5$. The activity is varied in the range $\alpha \in [0, 10^{-2}]$ and the phoretic mobilities in $\mu_\pm \in [0, 0.6]$ (we consider only oxyrepulsive particles). Correspondingly, the largest propulsion speeds attained are such that the particle scale Reynolds number ($Re = v_p R/\nu$), the Mach number ($Ma = v_p/c_s$, c_s being the speed of sound), and the Péclet number ($Pe = v_p R/D_\phi$) never exceed the values $Re \approx 0.1$, $Ma \approx 0.03$, and $Pe \approx 3$ (although in most of the simulations, we have $Pe \approx 0.1$), respectively, and thus, we are legitimately in an incompressible creeping flow regime.

Unless otherwise specified, the system is initialized with two slabs of oil and water separated by a flat interface (actually two due to the periodic boundary conditions), corresponding to the equilibrium hyperbolic tangent profile $\psi(\mathbf{r}, 0) = \tanh(x/\xi)$. The oxygen field is initially set to $\phi(\mathbf{r}, 0) = 0$, everywhere, and then let equilibrate.

III. RESULTS AND DISCUSSION

A. Motion of a Janus particle in a single phase fluid

As a validation of the model, we first consider the motion of an isolated active particle in the bulk of a single phase fluid ($A = E = \kappa = 0$ and $\psi = 0$, identically). Figure 3(a) reports the results of a set of simulations aimed at tuning the degradation rate k_d. We note, first of all, that the introduction of the sink term works as expected and a steady state is reached. The stationary value, $\langle \phi - \phi_0 \rangle_\infty$, will depend, of course, on both the particle activity and the degradation rate, as shown in Fig. 3(a). In particular, it grows with α and decreases with k_d. The presence of a linear degradation term implies that the concentration field does not decay purely algebraically with the distance from the source (the particle surface), but it is modulated by an exponential factor, $\phi(r) \sim e^{-r/\ell}/r$, with screening length $\ell = \sqrt{D_\phi/k_d}$. In the remainder of this paper, the value of the degradation rate is kept fixed to $k_d = 10^{-3}$, which gives a screening length of approximately one particle diameter, $\ell \approx 2R$.

In Fig. 3(b), we check the dependence of the particle speed on the phoretic mobilities at fixed activity $\alpha = 10^{-3}$, plotting v_p vs μ_- (the mobility value on the active side) for various values of mobility on the opposite cap, μ_+. As expected from the theoretical prediction [Eq. (7)], the speed grows linearly with μ_- (and μ_+). The linearity deteriorates a bit as $\mu_\pm$ increase, probably due to the fact that the Péclet number is also increasing and tends to approach unity [we recall that the result (7) is derived under the assumption of vanishing Pe[37,38]].

B. Inactive Janus particles at liquid–liquid interfaces

Before facing the problem of active particle motion, a needed preliminary step is to investigate the interaction of an inactive diffusiophoretic particle with the interface in order to analyze the competing effect of capillary and phoretic forces. To this aim, first we focus on a particle with $\alpha = 0$ and uniform phoretic mobility, $\mu_+ = \mu_- = \mu$, initially placed in oil, water, or at the interface, depending on whether it is hydrophobic ($\theta_c = 0°$), neutral ($\theta_c = 90°$), and hydrophilic ($\theta_c = 180°$), respectively. Because of the imbalance of capillary and phoretic forces, the particle will relax from its initial position toward or away from the interface. We then monitor its equilibrium position relative to the interface, $(X_{CM} - X_{int})/R$, as a function of μ and the oxygen solubility parameter E. The results are shown in Fig. 4. When particles are placed in the bulk of the oil or water phases, being the surrounding solute homogeneous, diffusiophoretic forces vanish and μ and E do not affect the particle motion.

Conversely, particles initially trapped at the interface are surrounded by an inhomogeneous solute field, and diffusiophoretic forces become relevant. In particular, the larger is the difference of solute concentration in the two phases (i.e., for growing $|E|$), the stronger are these forces and the further they push the particle away from the interface. At the same time, phoretic forces depend on the strength of the particle–solute interaction; therefore, increasing $|\mu|$ has the same effect as increasing $|E|$. More formally, at mechanical equilibrium, phoretic and capillary forces balance each other along the normal to the interface, that is, $F_{cap} = F_{ph}$. The phoretic force is proportional to the concentration gradient, $F_{ph} \sim -\mu \nabla \phi$; next to the interface, we can approximate ϕ with a linear profile, by virtue of $\phi = E \tanh(\psi) = E \tanh(-\tanh(x/\xi)) \approx -Ex/\xi$, such that the force

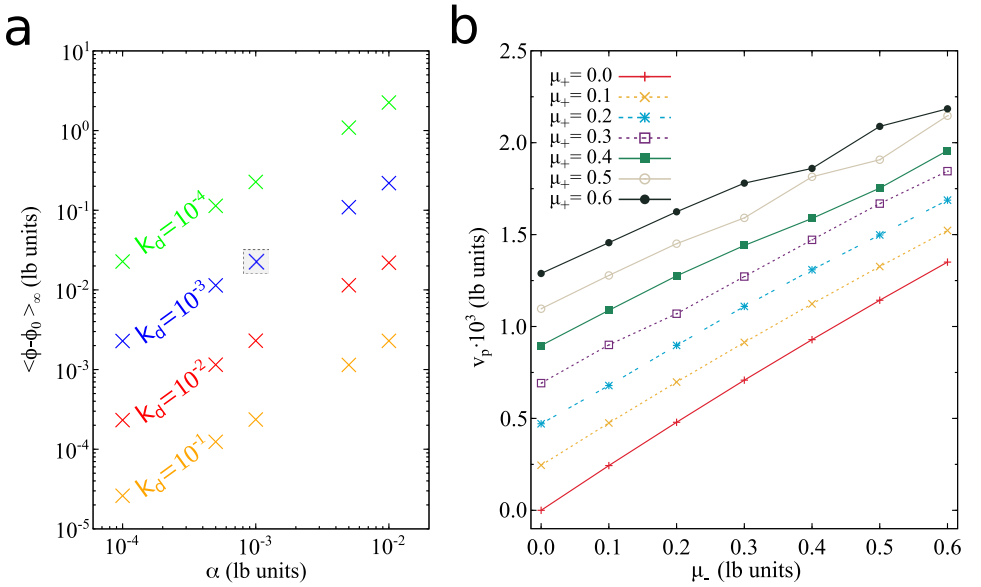

FIG. 3. Motion of an active Janus particle in a single phase fluid. (a) Steady state value of the space-averaged increase (with respect to the initial time) of oxygen concentration, $\langle \phi - \phi_0 \rangle_\infty$, as a function of the production rate α (in lbu) for various degradation rates, k_d. The rest of the data shown in this paper were obtained from simulations with $\alpha = 10^{-3}$ and $k_d = 10^{-3}$. (b) Particle speed as a function of the phoretic mobility μ_- for different values of μ_+ [see Eq. (6)], showing a linear dependence as predicted by Eq. (7).

reads $F_{\rm ph} \approx \mu E/\xi \propto \mu E$. For small interface deformations, capillarity acts as a Hookean restoring force, with an effective elastic constant proportional to the surface tension,[41] i.e., $F_{\rm cap} \propto \sigma \Delta X$, hence

$$\Delta X \equiv X_{\rm CM} - X_{\rm int} \propto \frac{\mu E}{\sigma}, \tag{11}$$

which explains the behavior emerging from Fig. 4.

We next consider the case of inhomogeneous phoretic mobilities, $\mu_- \neq \mu_+$, when an oxygen concentration gradient is present at the interface, $E \neq 0$. We set $E = -0.5$, which leads to a larger oxygen concentration in the oil phase, and impose neutral wetting ($\theta_c = 90°$). The particle is initially placed at the interface and aligned with it, i.e., its characteristic vector $\hat{m}$ lies in the interface plane and it is, then, orthogonal to the concentration gradient, $\hat{m} \perp \nabla\phi$. Consequently, due to the phoretic mobility mismatch, the particle is subject to a torque. We will consider here, therefore, both the equilibrium displacement and the equilibrium orientation angle, θ, with respect to the interface as functions of μ_- for different μ_+ values.

As expected, Fig. 5(a) shows that the particle relaxes to a position progressively further from the interface as the phoretic mobilities are increased. Interestingly, though, the equilibrium position saturates at a finite distance from the interface when $\mu_- > \mu_+ > 0$. These observations are better understood looking at Fig. 5(b), where the equilibrium orientation angle θ is plotted. The phoretic torque induced rotation undergone by the particle is faster if the difference

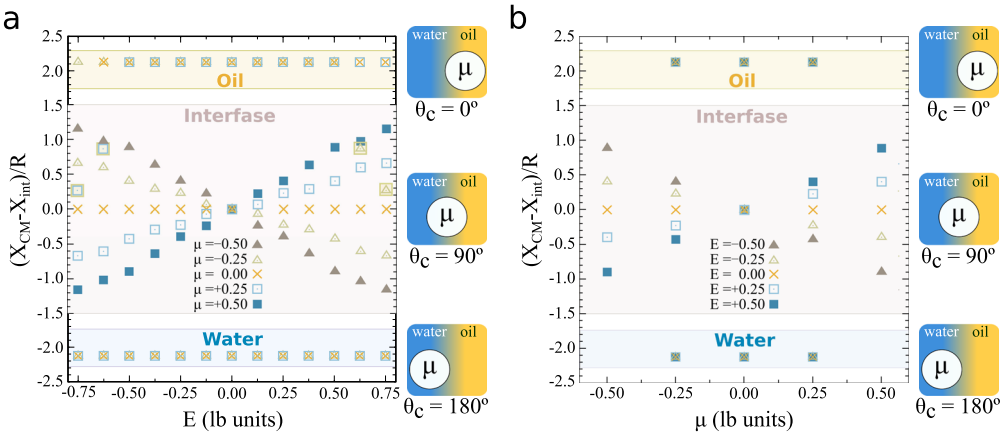

FIG. 4. Equilibrium position, relative to the interface, of an inactive ($\alpha = 0$) particle with uniform phoretic mobility as a function of E for various μ's [panel (a)] and as a function of μ for various E's [panel (b)]. Data for three different contact angles are shown; particles are initially placed in oil (hydrophobic, $\theta_c = 0°$), water (hydrophilic, $\theta_c = 180°$), or at the interface (neutral, $\theta_c = 90°$).

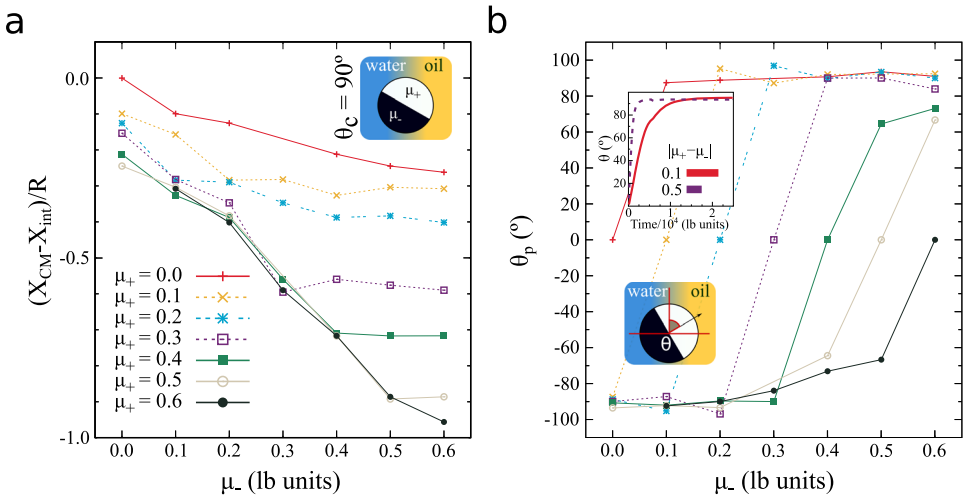

FIG. 5. Equilibrium position [panel (a)] and orientation angle [panel (b)] relative to the interface of an inactive particle ($\alpha = 0$) with a Janus phoretic mobility profile ($\mu_+ \neq \mu_-$) and neutral wetting ($\theta_c = 90°$) as a function of the rear mobility μ_- for various values of the front mobility μ_+. The particle, initially placed at the interface with the characteristic vector $\hat{m}$ in the interface plane, tends to escape from the plane by effect of phoretic repulsion and to rotate due to the mismatching mobilities inducing a torque [in the inset of panel (b), a typical time evolution of the orientation angle].

between both mobilities is larger, as expected [see inset of Fig. 5(b)]. Because particles reorient fast with the stronger phoretic mobility facing the water region, the side facing the oil is the more important input to displace the particle from the interface. Hence, this explains why in Fig. 5(a) we reach a saturation when $\mu_- > \mu_+$.

C. Active Janus particles and liquid–liquid interfaces

Once the inherent behavior of capillarity and wetting properties on passive Janus colloids has been established, we focus on the behavior of active Janus colloids, $\alpha \neq 0$, with a uniform phoretic mobility profile ($\mu_- = \mu_+ \equiv \mu$). Initially, we consider neutrally wetting particles trapped at the interface and analyze their motion at varying μ and the oxygen solubility parameter E, quantifying the product concentration ratio at the two sides of the interface. The values $\mu = 0.3$ and $\mu = 0.5$ and $E = -0.5$, $E = -0.25$, and $E = 0$ (corresponding to no concentration mismatch) are used. We run simulations starting with different particle orientations defined by θ_p, which is the angle between the particle characteristic vector and the interface (see Fig. 6).

When the difference of the product in the two phases is high ($E = -0.5$), Janus particles move along the interface. Interestingly, if the simulations are initialized with different θ_p, particles stabilize at a unique angle, which depends on the particle surface mobility. A theoretical explanation of the origin and precise values of these attractors is not easy due to the many different mechanisms that come into play: hydrodynamic torques, diffusiophoretic torques, and wetting particle–interface interaction. A qualitative argument can be provided, though, about the dependence of the steady state angle on the phoretic mobility. The existence of an equilibrium value suggests that the total torque acting on the particle must vanish. Among the various contributions to it, let us single out the phoretic torque, $\mathbf{T}_{ph}$. Due to the larger solubility of oxygen in the oil phase, when the particle is oriented with an angle θ_p with respect to the interface, the axial symmetry of the concentration profile around it is broken. A portion of the catalytic cap, in fact, is exposed to a region (within the oil phase) with more oxygen. As a consequence, the active hemisphere can be schematically divided in three sectors that contribute to the total torque as (an analogous expression can be written, by symmetry, for the inactive hemisphere)

$$T_{ph}(\theta) = \begin{cases} +T_0 & \text{if} \quad -\pi \le \theta < -\pi/2, \\ -(T_0 + \Delta T) & \text{if} \quad \pi/2 < \theta \le \pi - \theta_p, \\ -T_0 & \text{if} \quad \pi - \theta_p < \theta < \pi, \end{cases} \tag{12}$$

where a scalar form (piecewise constant for simplicity) is assumed since the problem is effectively two-dimensional. T_0 is the basic torque contribution due to the produced field, and ΔT is the excess torque to the solubility induced oxygen gradient at the interface. Both quantities, of course, are proportional to the phoretic mobility. The total torque will be, then,

$$T_{ph} = T_0 \frac{\pi}{2} - (T_0 + \Delta T)\left(\frac{\pi}{2} - \theta_p\right) - T_0\theta_p = -\Delta T\left(\frac{\pi}{2} - \theta_p\right). \tag{13}$$

The phoretic torque, then, tends to rotate the particle out of the interface. In particular, then, the larger $|\Delta T| \propto \mu$, the more the equilibrium angle approaches $\pi/2$, which agrees with the observation reported in the left panel of Fig. 6.

When the ratio of products in both phases is closer to 1 (e.g., $E = -0.25$), particles continue their motion at interfaces, although they are slower, and a unique angle is no longer observed. For some mobilities, as in $\mu = 0.3$, a single angle is observed, but for others, as for $\mu = 0.5$, we observe the appearance of competing attractors. Thus, both the asymmetric accumulation of the product in both sides and the surface mobility of the particle change the torque the particle feels at the interface and that stabilizes at a certain θ_p. Finally, in the last scenario where both phases are symmetric with respect to the solute solubility, $E = 0$, particles move very slowly along the interface, and additional attractors for θ_p appear. Consequently, the asymmetric accumulation of the product is also responsible for the particle speed at the interface.

We next analyze the impact of wetting when a particle is initially placed at the interface and moves along it. We consider both active and inactive particles and monitor the steady displacement of

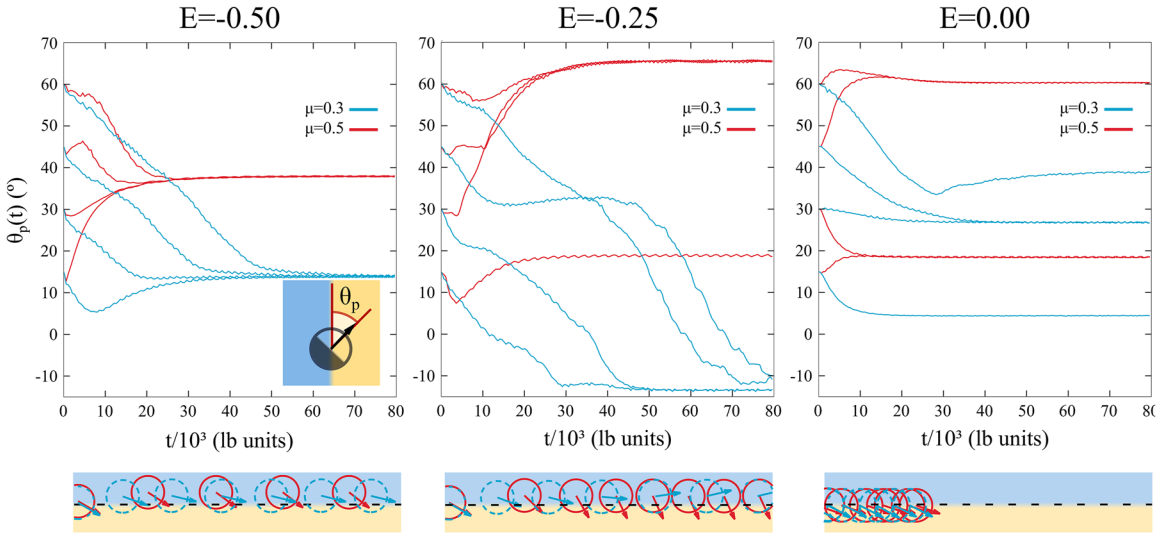

FIG. 6. Angle between the particle characteristic vector and the interface, θ_p, as a function of time for an active colloid with $\theta_c = 90°$ (neutral wetting), trapped at the interface. The datasets correspond to various initial orientation angles, two different surface mobilities ($\mu = 0.3$ and $\mu = 0.5$), and three different oxygen-oil/water affinities: $E = -0.5$ (left panel), $E = -0.25$ (middle panel), and $E = 0$ (right panel). The insets below the curves indicate the progression of the particles along the interface for the case with initial $\theta_p = 60°$ for the 8×10^4 time steps simulated.

the particle from the interface plane at changing the contact angle, the phoretic mobilities, and the oxygen solubility parameter. The results are reported in Fig. 7(a).

Inactive, non-phoretic ($\mu = 0$) particles are, of course, insensitive to variations of the oxygen field configuration and, hence, to E; this is reflected in the full overlap of the data for $E = 0$ (red plus) and $E = -0.5$ (orange cross). In both cases, though, as expected for passive colloids, the more the contact angle departs from 90°, the further the particle settles away from the interface.

Remarkably, instead, for finite, large enough phoretic mobility ($\mu = 0.5$), phoretic repulsion is capable to overcome interfacial forces and the particle tends to stay away from the phase richer in oxygen, be it water, $E > 0$ (pink empty square), or oil, $E < 0$ (blue asterisk), irrespective of its wettability. More precisely,

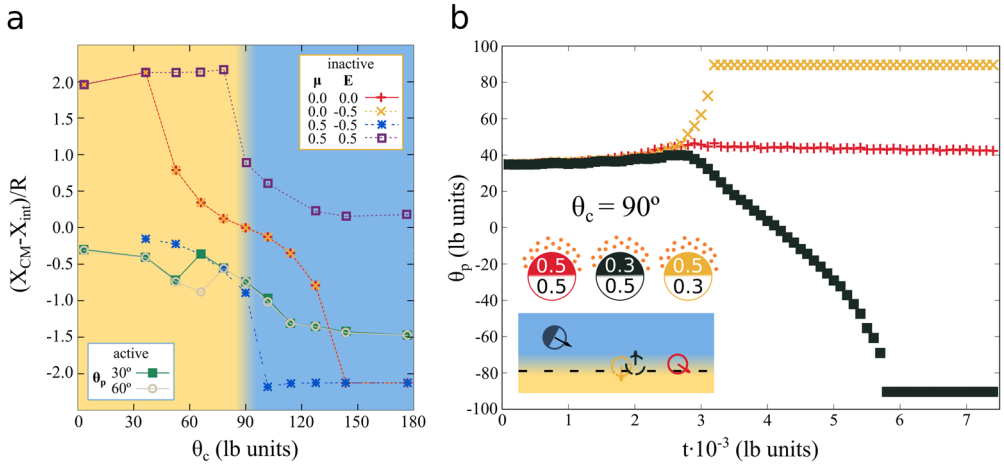

FIG. 7. (a) Steady particle displacement with respect to the interface as a function of the contact angle for various combinations of μ, E, and $\alpha = 0$ (inactive) or $\alpha = 10^{-3}$ (active). In the active case, data for two different values of the initial orientation angle are shown: $\theta_p^{(0)} = 30°$ (green filled square) and $\theta_p^{(0)} = 60°$ (gray empty circle). (b) Trajectory (in a plane orthogonal to the interface) of an active particle initially placed in water and oriented toward the interface (indicated with the dashed line); the initial orientation angle is $\theta = 30°$ and the colloid is neutral ($\theta_c = 90°$). Three combinations of phoretic mobilities (μ_+, μ_-) are considered: (0.5, 0.5) (red), (0.5, 0.3) (blue), and (0.3, 0.5) (green).

taking, for instance, the case $E < 0$, if phoretic and capillary forces have opposite directions ($\theta_c < 90°$), the particle can be stabilized, roughly, at the interface, but if they point toward the same side, the particle leaves the interface plane and there is, basically, no dependence on the contact angle.

Active particles ($\alpha \neq 0$), for which only the case $E < 0$ is shown, manifest a similar behavior. However, the activity introduces an extra force that has a component normal to the interface (for the steady orientation angle differs, in general, from zero) and pushes the particle closer to the oxygen-rich region. To check if the initial orientation $\theta_p^{(0)}$ plays a role, simulations are run with $\theta_p^{(0)} = 60°$ (green filled square) and $\theta_p^{(0)} = 30°$ (gray filled square). The absence of significant differences indicates that $\theta_p^{(0)}$ does not impact the steady state particle motion.

Finally, we study the motion of neutral ($\theta_c = 90°$) active particles that approach the interface from the aqueous phase when the oxygen is more concentrated in oil ($E < 0$), as displayed in Fig. 7(b). We consider both uniform ($\mu_+ = \mu_- = \mu = 0.5$, red) and Janus-like phoretic mobilities [$\mu_+ = 0.5$, $\mu_- = 0.3$ (black) and $\mu_+ = 0.3$, $\mu_- = 0.5$ (yellow)].

Janus particles tend to reorient such to minimize the interfacial overlap of the more repulsive side (larger μ) with the solute-rich liquid. Thus, the particle with higher front mobility ($\mu_+ > \mu_-$, in black) faces the water phase (depicted as a blue area in the inset), attaining a value of the orientation angle $\theta_p \approx -90°$, whereas the opposite occurs when $\mu_+ < \mu_-$ ($\theta_p \approx 90°$, in yellow). In both cases, since their director vector $\hat{m}$ is orthogonal to the interface and phoretic forces cannot overcome the capillary trapping, they get stuck. On the contrary, for uniform diffusiophoretic mobilities (red particle), orthogonal interfacial alignment is lacking, and particles displace along the interface.

IV. CONCLUSIONS

In this work, we have introduced a new model based on the lattice Boltzmann method to study the interaction of active particles with liquid–liquid interfaces. The model facilitates the study of the full hydrodynamics of the system, on the same footing as diffusiophoretic and wetting forces suspended particles are subject to. The model allows us to switch on and off easily these forces and to modify the particle properties, such as wetting and the diffusiophoretic forces, differentiating for this last scenario two parts on the particle with its own activity and mobility. These contributions are formulated locally and can then be adapted to particles of arbitrary shape, with a general inhomogeneous treatment of their surfaces. Moreover, the liquid mixture can show asymmetric solubility to the chemicals produced by the particles.

We have tested the interaction of inactive particles trapped at the interface under different wetting angles θ_c (0°, 90°, and 180°) and different particle surface mobilities. We have seen that while wetting dominates over diffusiophoretic forces, when the wetting is neutral (90°), diffusiophoretic properties are important, and inactive particles with homogeneous surface mobility displace from the interface. This interaction is proportional to the surface mobility and to the different of products between both phases. When the surface has an asymmetric mobility, particles reorient to have their more repulsive face toward the liquid phase with less product and displace from the phase of high accumulation of product. The reorientation depends on the strength of the mobility. The more repulsive the particles are, the faster they reorient.

Active particles at the interface with neutral wetting move along the interface. The larger the asymmetry between product accumulation in both phases and the more repulsive is their surface to products, the faster the particles move. Particles reorient themselves to a specific angle, no matter the angle at which particles are placed. However, if the asymmetry of products between both phases is reduced, particles find different equilibrium positions depending on the initial angle. This effect is seen for different surface mobilities. Hydrophobic and hydrophilic active particles tend to stay closer to the interface than their passive counterparts. Particles initially placed in a fluid, for which they have high affinity, and moving towards the interface will eventually touch it, rotate and displace along it. Depending on the ratio of the surface mobilities, particles can stop or continue their motion.

Overall, the proposed model has huge capabilities to explain many phenomena occurring at these interfaces, and that sets a new start line where to study these and more complex systems.

ACKNOWLEDGMENTS

L.S.P. would like to acknowledge MINECO for the FPI BES-2016-077705 fellowship. A.S. acknowledges support from the European Research Council under the European Union Horizon 2020 Framework Program (No. FP/2014-2020), ERC Grant Agreement No. 739964 (COPMAT). I.P. acknowledges support from Ministerio de Ciencia, Innovación y Universidades (Grant No. PGC2018-098373-B-100/FEDER-EU), DURSI (Grant No. 2017 SGR 884), SNSF (Project No. 200020$_2$04671), and the European Union Horizon 2020 Program (Grant No. FET-OPEN 766972-NANOPHLOW).

AUTHOR DECLARATIONS

Conflict of Interest

The authors have no conflicts to disclose.

DATA AVAILABILITY

The data that support the findings of this study are available from the corresponding author upon reasonable request.

REFERENCES

[1] S. Sánchez, L. Soler, and J. Katuri, "Chemically powered micro- and nanomotors," Angew. Chem., Int. Ed. **54**, 1414–1444 (2015).
[2] S. Ramaswamy, "The mechanics and statistics of active matter," Annu. Rev. Condens. Matter Phys. **1**, 323–345 (2010).
[3] J. L. Anderson, "Colloid transport by interfacial forces," Annu. Rev. Fluid Mech. **21**, 61–99 (1989).
[4] W. F. Paxton, K. C. Kistler, C. C. Olmeda, A. Sen, S. K. St. Angelo, Y. Cao, T. E. Mallouk, P. E. Lammert, and V. H. Crespi, "Catalytic nanomotors: Autonomous movement of striped nanorods," J. Am. Chem. Soc. **126**, 13424–13431 (2004).
[5] J. R. Howse, R. A. L. Jones, A. J. Ryan, T. Gough, R. Vafabakhsh, and R. Golestanian, "Self-motile colloidal particles: From directed propulsion to random walk," Phys. Rev. Lett. **99**, 048102 (2007).

[6]I. Theurkauff, C. Cottin-Bizonne, J. Palacci, C. Ybert, and L. Bocquet, "Dynamic clustering in active colloidal suspensions with chemical signaling," Phys. Rev. Lett. **108**, 268303 (2012).
[7]G. Volpe, I. Buttinoni, D. Vogt, H.-J. Kümmerer, and C. Bechinger, "Microswimmers in patterned environments," Soft Matter **7**, 8810–8815 (2011).
[8]J. Palacci, S. Sacanna, A. P. Steinberg, D. J. Pine, and P. M. Chaikin, "Living crystals of light-activated colloidal surfers," Science **339**, 936–940 (2013).
[9]W. F. Paxton, S. Sundararajan, T. E. Mallouk, and A. Sen, "Chemical locomotion," Angew. Chem., Int. Ed. **45**, 5420–5429 (2006).
[10]S. J. Ebbens and J. R. Howse, "In pursuit of propulsion at the nanoscale," Soft Matter **6**, 726–738 (2010).
[11]C. Bechinger, R. Di Leonardo, H. Löwen, C. Reichhardt, G. Volpe, and G. Volpe, "Active particles in complex and crowded environments," Rev. Mod. Phys. **88**, 045006 (2016).
[12]I. Buttinoni, J. Bialké, F. Kümmel, H. Löwen, C. Bechinger, and T. Speck, "Dynamical clustering and phase separation in suspensions of self-propelled colloidal particles," Phys. Rev. Lett. **110**, 238301 (2013).
[13]R. Golestanian, "Collective behavior of thermally active colloids," Phys. Rev. Lett. **108**, 038303 (2012).
[14]M. Yang, A. Wysocki, and M. Ripoll, "Hydrodynamic simulations of self-phoretic microswimmers," Soft Matter **10**, 6208–6218 (2014).
[15]J. Simmchen, J. Katuri, W. E. Uspal, M. N. Popescu, M. Tasinkevych, and S. Sánchez, "Topographical pathways guide chemical microswimmers," Nat. Commun. **7**, 10598 (2016).
[16]J. Katuri, D. Caballero, R. Voituriez, J. Samitier, and S. Sanchez, "Directed flow of micromotors through alignment interactions with micropatterned ratchets," ACS Nano **12**, 7282–7291 (2018).
[17]W. E. Uspal, M. N. Popescu, S. Dietrich, and M. Tasinkevych, "Self-propulsion of a catalytically active particle near a planar wall: From reflection to sliding and hovering," Soft Matter **11**, 434–438 (2015).
[18]A. Domínguez, P. Malgaretti, M. N. Popescu, and S. Dietrich, "Effective interaction between active colloids and fluid interfaces induced by marangoni flows," Phys. Rev. Lett. **116**, 078301 (2016).
[19]P. Malgaretti, M. N. Popescu, and S. Dietrich, "Active colloids at fluid interfaces," Soft Matter **12**, 4007–4023 (2016).
[20]X. Wang, M. In, C. Blanc, P. Malgaretti, M. Nobili, and A. Stocco, "Wetting and orientation of catalytic Janus colloids at the surface of water," Faraday Discuss. **191**, 305–324 (2016).
[21]T. Peter, P. Malgaretti, N. Rivas, A. Scagliarini, J. Harting, and S. Dietrich, "Numerical simulations of self-diffusiophoretic colloids at fluid interfaces," Soft Matter **16**, 3536–3547 (2020).
[22]L. S. Palacios, J. Katuri, I. Pagonabarraga, and S. Sánchez, "Guidance of active particles at liquid–liquid interfaces near surfaces," Soft Matter **15**, 6581–6588 (2019).
[23]R. Benzi, S. Succi, and M. Vergassola, "The lattice Boltzmann equation: Theory and applications," Phys. Rep. **222**, 145–197 (1992).
[24]D. Wolf-Gladrow, *Lattice-Gas Cellular Automata and Lattice Boltzmann Models: An Introduction* (Springer, 2000).
[25]T. Krüger, H. Kusumaatmaja, A. Kuzmin, O. Shardt, G. Silva, and E. Viggen, *The Lattice Boltzmann Method* (Springer, 2017).
[26]F. Bonaccorso, A. Montessori, A. Tiribocchi, G. Amati, M. Bernaschi, M. Lauricella, and S. Succi, "LBsoft: A parallel open-source software for simulation of colloidal systems," Comput. Phys. Commun. **256**, 107455 (2020).
[27]M. R. Swift, E. Orlandini, W. R. Osborn, and J. M. Yeomans, "Lattice Boltzmann simulations of liquid-gas and binary fluid systems," Phys. Rev. E **54**, 5041–5052 (1996).
[28]V. M. Kendon, M. E. Cates, I. Pagonabarraga, J.-C. Desplat, and P. Bladon, "Inertial effects in three-dimensional spinodal decomposition of a symmetric binary fluid mixture: A lattice Boltzmann study," J. Fluid Mech. **440**, 147–203 (2001).
[29]L. N. Carenza, G. Gonnella, A. Lamura, G. Negro, and A. Tiribocchi, "Lattice Boltzmann methods and active fluids," Eur. Phys. J. E **42**, 81 (2019).
[30]J. W. Cahn and J. E. Hilliard, "Free energy of a nonuniform system. I. Interfacial free energy," J. Chem. Phys. **28**, 258–267 (1958).
[31]A. Scagliarini and I. Pagonabarraga, "Unravelling the role of phoretic and hydrodynamic interactions in active colloidal suspensions," Soft Matter **16**, 8893–8903 (2020).
[32]A. J. C. Ladd, "Numerical simulations of particulate suspensions via a discretized Boltzmann equation. Part 1. Theoretical foundation," J. Fluid Mech. **271**, 285–309 (1994).
[33]A. J. C. Ladd, "Numerical simulations of particulate suspensions via a discretized Boltzmann equation. Part 2. Numerical results," J. Fluid Mech. **271**, 311–339 (1994).
[34]N.-Q. Nguyen and A. J. C. Ladd, "Lubrication corrections for lattice-Boltzmann simulations of particle suspensions," Phys. Rev. E **66**, 046708 (2002).
[35]C. K. Aidun, Y. Lu, and E.-J. Ding, "Direct analysis of particulate suspensions with inertia using the discrete Boltzmann equation," J. Fluid Mech. **373**, 287–311 (1998).
[36]F. Bonaccorso, S. Succi, M. Lauricella, A. Montessori, A. Tiribocchi, and K. H. Luo, "Shear dynamics of confined bijels," AIP Adv. **10**, 095304 (2020).
[37]R. Golestanian, T. B. Liverpool, and A. Ajdari, "Designing phoretic micro- and nano-swimmers," New J. Phys. **9**, 126 (2007).
[38]R. Golestanian, T. B. Liverpool, and A. Ajdari, "Propulsion of a molecular machine by asymmetric distribution of reaction products," Phys. Rev. Lett. **94**, 220801 (2005).
[39]M. N. Popescu, S. Dietrich, M. Tasinkevych, and J. Ralston, "Phoretic motion of spheroidal particles due to self-generated solute gradients," Eur. Phys. J. E **31**, 351–367 (2010).
[40]J.-C. Desplat, I. Pagonabarraga, and P. Bladon, "LUDWIG: A parallel Lattice-Boltzmann code for complex fluids," Comput. Phys. Commun. **134**, 273–290 (2001).
[41]J. F. Joanny and P. G. de Gennes, "A model for contact angle hysteresis," J. Chem. Phys. **81**, 552–562 (1984).